11. F. V. Kaminsky, S. M. Sablukov, L. I. Sablukova, V. E. Shpanov. *Izvestya (Earth Science Section)* **4**, 85 (2000).
12. D. H. Robinson, in *The Mantle Sample: Inclusions in Kimberlites and Other Volcanics*, F. R. Boyd, H. O. A. Meyer, Eds. (American Geophysical Union, Washington, DC, 1979), pp. 50–58.
13. D. H. Robinson, J. A. Scott, A. Van Nierkerk, V. G. Anderson, in *Kimberlites and Related Rocks: Their Mantle/Crust Settings, Diamonds and Diamond Exploration*, J. Ross *et al.* Eds. (Blackwell, Oxford, UK, 1989), vol. 2, pp. 991–1000.
14. G. S. Woods, A. T. Collins, *J. Phys. Chem. Solids* **44**, 471 (1983).
15. O. Navon, I. D. Hutcheon, G. R. Rossman, G. J. Wasserburg, *Nature* **355**, 784 (1988).
16. $\delta^{13}C = [(^{13}C/^{12}C_{sample})/(^{13}C/^{12}C_{PDB}) - 1] \times 1000$, where PDB is Pee Dee Belemnita. Twenty-eight samples were combusted for $\delta^{13}C$ solely at Queen's University (Kingston, Ontario, Canada) with the use of elemental analyser–ion ratio mass spectrometry (EA-IRMS) technique, whereas the 20 others were obtained together with $\delta^{15}N$ and N content measurements at Institut de Physique du Globe de Paris (IPGP), Paris (*17*, *43*).
17. S. R. Boyd, A. Réjou-Michel, M. Javoy, *Meas. Sci. Technol.* **6**, 297 (1995).
18. S. H. Richardson, J. J. Gurney, A. J. Erlank, J. W. Harris, *Nature* **310**, 198 (1984).
19. J. W. Harris, in *The Properties of Natural and Synthetic Diamond*, J. E. Field, Ed. (Academic Press, London, 1992), pp. 345–394.
20. R. M. Davies *et al.*, in *Proceedings of the 7th International Kimberlite Conference*, J. J. Gurney, J. L. Gurney, M. D. Pascoe, S. H. Richardson, Eds. (Red Roof Design, Cape Town, South Africa, 1999), pp. 148–155.
21. P. Deines, J. W. Harris, J. J. Gurney, *Geochim. Cosmochim. Acta* **61**, 3993 (1997).
22. P. Cartigny, S. R. Boyd, J. W. Harris, M. Javoy, *Terra Nova* **9**, 175 (1997).
23. T. Stachel, J. W. Harris, R. Tappert, G. P. Brey, *Lithos* **71**, 489 (2003).
24. H. B. Dyer, F. A. Raal, L. Du Preez., J. H. N. Loubser, *Philos. Mag.* **11**, 763 (1965).
25. P. Cartigny, J. W. Harris, A. Taylor, R. M. Davies, M. Javoy, *Geochim. Cosmochim. Acta* **67**, 1571 (2003).
26. T. Evans, Z. Qi, *Proc. R. Soc. London Ser. A* **381**, 159 (1982).
27. W. R. Taylor, D. Canil, H. J. Milledge, *Geochim. Cosmochim. Acta* **60**, 4725 (1996).
28. R. L. Trautman *et al.*, *Russ. Geol. Geophys.* **38**, 341 (1997).
29. M. Schrauder, thesis, University of Wien, Austria (1997).
30. S. R. Boyd, F. Pineau, M. Javoy, *Chem. Geol.* **116**, 29 (1994).
31. R. M. Davies, W. L. Griffin, S. Y. O'Reilly, B. J. Doyle, abstract FL048, presented at the 8th International Kimberlite Conference, Victoria, Canada, 22 to 27 June 2003.
32. M. E. McCallum, C. D. Mabarak, H. G. Coppersmith, in *Diamonds: Characterization, Genesis, and Exploration*, H. O. A. Meyer, O. H. Leonardos, Eds. [Companhia de Pesquisa de Recursos Minerais (CPRM) Special Publication, Araxa, Brazil, 1991], pp. 32–50.
33. T. E. McCandless, M. A. Waldman, J. J. Gurney, in *Diamonds: Characterization, Genesis, and Exploration*, H. O. A. Meyer, O. H. Leonardos, Eds. (CPRM Special Publication, Araxa, Brazil, 1991), pp. 78–97.
34. D. A. Shelkov *et al.*, *Source Meteorit. Planet. Sci.* **33**, 985 (1998).
35. E. M. Galimov, F. V. Kaminsky, L. A. Kodina, *Geochem. Int.* **22**, 18 (1985).
36. S. T. Xu *et al.*, *Science* **256**, 80 (1992).
37. L. F. Dobrzhinetskaya *et al.*, *Geology* **23**, 597 (1995).
38. K. S. Finnie, D. Fisher, W. L. Griffin, J. W. Harris, N. V. Sobolev, *Geochim. Cosmochim. Acta* **58**, 5173 (1994).
39. K. De Corte, P. Cartigny, V. S. Shatsky, N. V. Sobolev, M. Javoy, *Geochim. Cosmochim. Acta* **62**, 3765 (1998).
40. K. De Corte *et al.*, in *Proceedings of the 7th International Kimberlite Conference*, J. J. Gurney, J. L. Gurney, M. D. Pascoe, S. H. Richardson, Eds. (Red Roof Design, Cape Town, South Africa, 1999), pp. 174–182.
41. V. Beaumont, F. Robert, *Precambrian Res.* **96**, 63 (1999).
42. B. Mingram, K. Bräuer, *Geochim. Cosmochim. Acta* **65**, 273 (2001).
43. P. Cartigny *et al.*, *Chem. Geol.* **176**, 267 (2001).
44. B. Stoeckhert, J. Duyster, C. Trepmann, H.-J. Massonne, *Geology* **29**, 391 (2001).
45. G. Zhao, P. A. Cawood, S. A. Wilde, M. Sun, *Earth Sci. Rev.* **59**, 125 (2002).
46. M. G. Bardet, *Géologie du Diamant III, Mémoires du BRGM* (Editions du Bureau de Recherches Géologiques et Minières, Paris, 1977), p. 166.
47. I. Chinn, P. Cartigny, unpublished data.
48. S. R. Boyd *et al.*, *Earth Planet. Sci. Lett.* **86**, 341 (1987).
49. S. R. Boyd, C. T. Pillinger, H. J. Milledge, M. J. Mendelssohn, M. Seal, *Earth Planet. Sci. Lett.* **109**, 663 (1992).
50. P. Cartigny, unpublished data.
51. The paper benefited from constructive comments by two reviewers and by J. W. Harris, C. Aubaud, V. Busigny, and B. McKechnie on a preliminary version of this article. J. Dyon is thanked for fig. S1 and K. Kyser for $\delta^{13}C$ data obtained by EA-IRMS. The authors thank management of De Beers Consolidated Mines Limited for donation of study material and permission to publish. IPGP contribution 1969.

Post-Perovskite Phase Transition in MgSiO₃

Motohiko Murakami,[1]* Kei Hirose,[1]* Katsuyuki Kawamura,[1] Nagayoshi Sata,[2] Yasuo Ohishi[3]

In situ x-ray diffraction measurements of MgSiO₃ were performed at high pressure and temperature similar to the conditions at Earth's core-mantle boundary. Results demonstrate that MgSiO₃ perovskite transforms to a new high-pressure form with stacked SiO₆-octahedral sheet structure above 125 gigapascals and 2500 kelvin (2700-kilometer depth near the base of the mantle) with an increase in density of 1.0 to 1.2%. The origin of the D″ seismic discontinuity may be attributed to this post-perovskite phase transition. The new phase may have large elastic anisotropy and develop preferred orientation with platy crystal shape in the shear flow that can cause strong seismic anisotropy below the D″ discontinuity.

MgSiO₃ perovskite is believed to be a principal mineral, at least in the upper part of the lower mantle, but its stability and possible phase transition at greater depths remain uncertain. Because seismic observations have shown unexplained features in the lowermost mantle (*1–4*), solid-solid phase transitions that could occur in this region are a subject of debate. Previous experiments have confirmed the conservation of orthorhombic (Mg, Fe)SiO₃ perovskite (space group: *Pbnm*) up to 127 GPa (*5–7*), consistent with first-principles total energy calculations (*8–10*). In contrast, an experimental study by Shim *et al.* (*11*) suggested a subtle change in the perovskite structure above 83 GPa and 1700 K. The dissociation of MgSiO₃ into mixed oxides was also previously found at 70 to 80 GPa (*12*, *13*), but it was possibly due to melting or diffusion caused by a large temperature gradient in these earlier studies (*14*). Here we report in situ x-ray observation of pure MgSiO₃ composition at high pressure and temperature up to 134 GPa and 2600 K corresponding to the conditions at the core-mantle boundary region.

Angle-dispersive x-ray diffraction (XRD) spectra were collected at BL10XU of SPring-8 (*15*). High-pressure and -temperature conditions were generated in a laser-heated diamond anvil cell (LHDAC) (*16*). MgSiO₃ gel was used as a starting material. It was mixed with platinum powder that served both as an internal pressure standard and a laser absorber. The sample mixture (~25 μm thick) was loaded into a 60-μm hole drilled in the rhenium gasket together with insulation layers of MgSiO₃ gel unmixed with platinum (~10 μm thick on both sides). They were compressed with 200-μm culet beveled diamond anvils. Heating was achieved by a focused multimode continuous-wave Nd: yttrium-aluminum-garnet laser using the double-side heating technique (*17*), which minimizes radial and axial temperature gradient in the sample (*18*). A heating spot was about 50 μm in diameter. Temperature was measured from one side by the spectroradiometric method (*19*). The uncertainty in temperature

[1]Department of Earth and Planetary Sciences, Tokyo Institute of Technology, 2-12-1 Ookayama, Meguro, Tokyo 152-8551, Japan. [2]Institute for Frontier Research on Earth Evolution, Japan Agency for Marine-Earth Science and Technology, 2-15 Natsushima-cho, Yokosuka, Kanagawa 237-0061, Japan. [3]Japan Synchrotron Radiation Research Institute, 1-1-1 Mikazuki-cho, Sayo-gun, Hyogo 679-5198, Japan.

*To whom correspondence should be addressed. E-mail: mmurakam@geo.titech.ac.jp (M.M.); kei@geo.titech.ac.jp (K.H.)

within the 20-μm area from which XRD spectra were collected was about ±200 K. Pressure was determined using the equation of state of platinum (20) with both (111) and (200) lines. The uncertainty in pressure was ±1.6 to 3.9 GPa, derived mainly from the uncertainty in temperature in the application of P-V-T equation of state. We conducted two separate sets of experiments. The diffraction patterns of the sample were repeatedly obtained at high temperatures during heating and at room temperature after quenching.

In the first run, an amorphous sample was compressed to 124 GPa at room temperature and then heated to 2250 to 2300 K for 11 min at 105 to 114 GPa. The diffraction peaks of orthorhombic perovskite (Pbnm) appeared within 2 min and did not change with further heating. All peaks were indexed by the Pbnm perovskite and platinum (Fig. 1A). We further compressed this sample to 127 GPa at room temperature and reheated it to 2500 to 2600 K for 70 min at 127 to 134 GPa. Eleven new peaks appeared within 9 min. These new peaks grew, and peaks from perovskite became

weak with further heating (Fig. 1B). Two-dimensional diffraction images showed circular Debye rings for these new peaks (fig. S1). The consistency of the unit-cell parameters of platinum calculated respectively from (111) and (200) lines indicated that nonhydrostatic stress in the sample was not large after heating in these experiments. The St values—the multiplication of the elastic anisotropy factor S and the uniaxial stress component t—were 0.0010 to 0.0037 at 121 GPa and 300 K (21). The deviatoric stress should have been reduced because of a decrease in the sample volume when perovskite was first synthesized from the gel starting material (22).

In the second set of experiments, perovskite was first synthesized from the amorphous starting material by heating to 1700 to 1970 K for 15 min at 69 to 73 GPa. We then compressed this sample to 122 GPa at room temperature. With heating to 2200 to 2300 K at 128 to 129 GPa, intermittently for a total of 120 min by opening/closing the laser shutter several times at fixed press load, the new peaks were again observed in the diffraction

patterns within 10 min of heating and were the same as those in the first run. This sample was then decompressed to 97 GPa at room temperature. The new peaks were still recognized after decompression, although they had broadened (Fig. 1C). After heating to 2000 to 2200 K for 10 min at 89 to 101 GPa, the new peaks disappeared and the diffraction pattern changed back to that consisting only of Pbnm perovskite and platinum (Fig. 1D).

These new peaks do not correspond to the possible dissociation products of MgO or high-pressure polymorphs of SiO_2 (Fig. 1B). Shim et al. (11) observed one additional peak in the diffraction pattern of $MgSiO_3$ perovskite and suggested a minor structural change. This extra peak, however, was not found in this study. These new peaks indicate that $MgSiO_3$ perovskite does not dissociate, but is transformed to a new high-pressure form above 125 GPa and 2500 K (Fig. 2). Phase transition in SiO_2 from a $CaCl_2$-type to a α-PbO_2–type structure, which occurs at similar pressure and temperature conditions (16), did not induce the dissociation of $MgSiO_3$. Xiong et al. (23) reported the phase
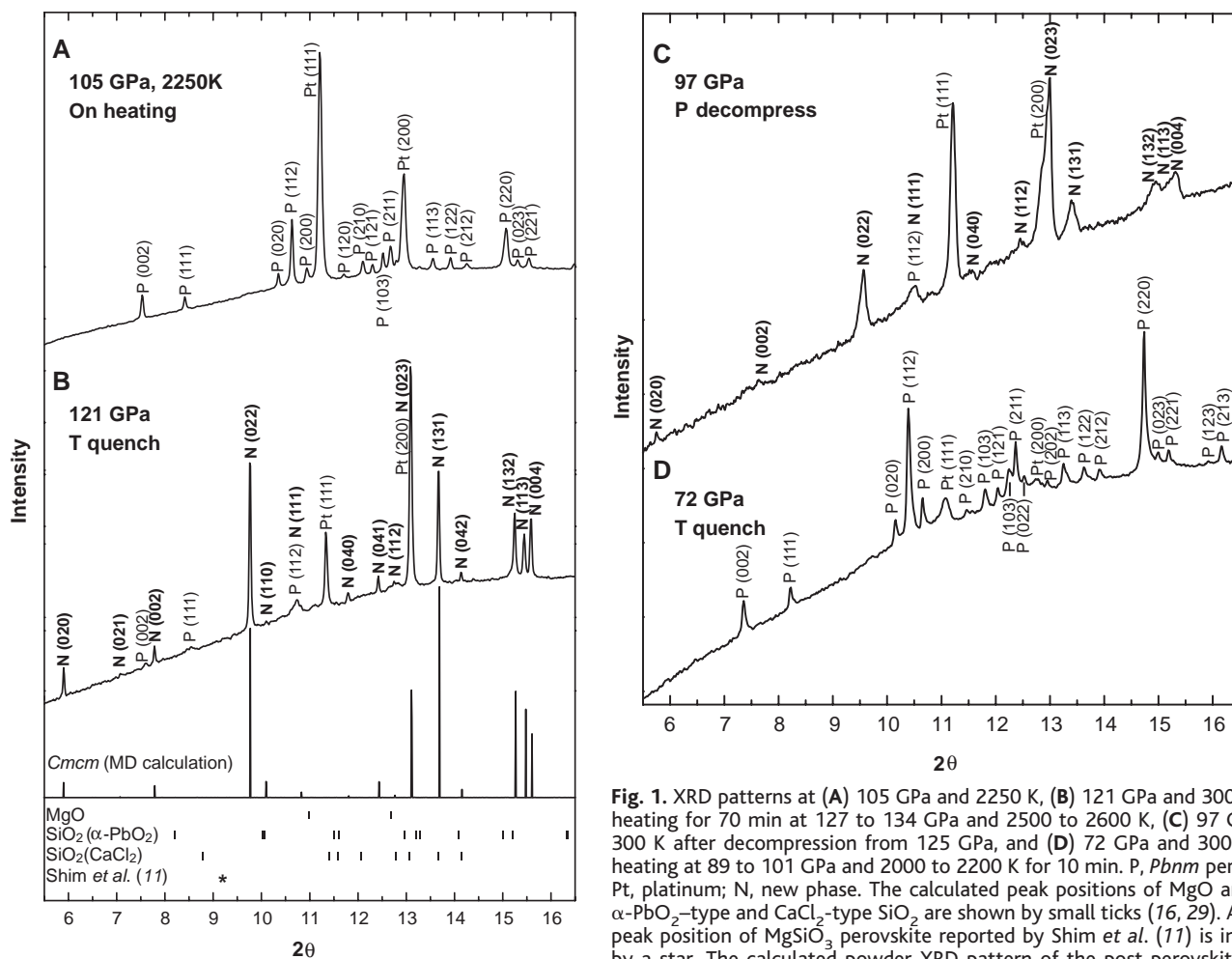

Fig. 1. XRD patterns at (**A**) 105 GPa and 2250 K, (**B**) 121 GPa and 300 K after heating for 70 min at 127 to 134 GPa and 2500 to 2600 K, (**C**) 97 GPa and 300 K after decompression from 125 GPa, and (**D**) 72 GPa and 300 K after heating at 89 to 101 GPa and 2000 to 2200 K for 10 min. P, Pbnm perovskite; Pt, platinum; N, new phase. The calculated peak positions of MgO and both α-PbO_2–type and $CaCl_2$-type SiO_2 are shown by small ticks (16, 29). An extra peak position of $MgSiO_3$ perovskite reported by Shim et al. (11) is indicated by a star. The calculated powder XRD pattern of the post-perovskite phase was corrected for Lorentz, polarization, and multiplicity factors to compare with the observed pattern.

transition of CaTiO$_3$ perovskite (*Pbnm*) to hexagonal and tetragonal structures when the pressure was increased to 10 to 15 GPa. However, we failed to assign the new peaks to these structures. Alternatively, the diffraction peaks of a new MgSiO$_3$ polymorph can be indexed by an orthorhombic cell with lattice parameters a = 2.456(0) Å, b = 8.042(1) Å, and c = 6.093(0) Å.

In order to determine the crystal structure that possesses these lattice parameters, we conducted a molecular dynamics (MD)–aided crystal structure design. The appropriate number of atoms [8 Mg + 8 Si + 24 O; Z = 8 (number of formula unit) for a double unit cell because of the small *a*-parameter] were positioned randomly in the cell with the experimentally observed dimensions. Classical MD calculations were carried out with the (NVT) ensemble of this system at high temperature (5000 K), and then the system was quenched to 0 K (*24*) (table S1). We repeated the calculations, each time checking and correcting the atomic positions until the crystal structure became consistent with the crystal chemistry and the calculated XRD pattern matched the observed one. The result revealed a new crystal structure with space group *Cmcm* (Fig. 3). The crystal data of this post-perovskite phase are presented in Table 1. The calculated powder XRD pattern reproduces both peak po-

sitions and intensities of all the observed new peaks (Fig. 1B). We obtained a room-temperature density of 5.536 g/cm^3 for the observed new phase at 121 GPa. It is denser than perovskite coexisting in the diffraction pattern by 1.0 to 1.2% at 300 K. The MD calculations also showed smaller molar volumes for the post-perovskite phase (fig. S2).

This new MgSiO$_3$ polymorph has sixfold Si and eightfold Mg coordination, and the SiO$_6$-octahedra share the edges to make an octahedral chain like that of a rutile-type structure (Fig. 3). These chains run along the *a* axis and are interconnected by apical O atoms in the direction of the *c* axis to form edge and apex shared octahedral sheets. The octahedral sheets are stacked along the *b* axis with interlayer Mg^{2+} ions. The MD calculations suggest that the *b* axis is more compressible than are the *a* and *c* axes (fig. S2), and this compression behavior differs from that of *Pbnm* perovskite (*25*). The crystal structure of the post-perovskite phase is isostructural with UFeS$_3$ (*26*).

Phase transition of MgSiO$_3$-rich perovskite can cause large seismic heterogeneities in the lowermost mantle. The D″ discontinuity is observed in many regions around the world about 200 to 300 km above the core-mantle boundary (119 to 125 GPa) with a velocity increase of ~3% (*3*), although its

ubiquitous occurrence is still a subject of debate (*4*, *27*). The post-perovskite phase transition occurs at depths matching those of the D″ discontinuity (Fig. 2). Although the effects of minor elements such as FeO, Fe$_2$O$_3$, and Al$_2$O$_3$ at the transition pressure remain to be evaluated, this phase transition may be responsible for the D″ seismic discontinuity. A variation in the depth of the discontinuity could be due to a large effect of temperature on phase transition pressure. Sidorin *et al*. (*4*) previously proposed a hypothetical transition boundary with a Clapeyron slope of about 6 MPa/K, assuming that the D″ discontinuity is caused by a solid-solid phase transition. Although the Clapeyron slope is not well constrained from the present results, their supposed boundary is consistent with our data (Fig. 2). Masters and Gubbins (*28*) recently found the excess density of 0.4% in the bottom 500 km of the lower mantle. An expected density increase of 1.0 to 1.2% for the bottom ~200- to 300-km layer owing to the post-MgSiO$_3$ perovskite transition is consistent with their observations.

The high compressibility of the *b* axis compared to the *a* and *c* axes of the post-

Fig. 2. Phase diagram of MgSiO$_3$. Solid squares and open circles indicate the stabilities of *Pbnm* perovskite and post-perovskite phase, respectively. A broken line shows the transition boundary proposed by Sidorin *et al*. (*4*) to explain the D″ discontinuity by a solid-solid phase transition.

Table 1. Crystal data of the post-perovskite phase at 121 GPa and 300 K.

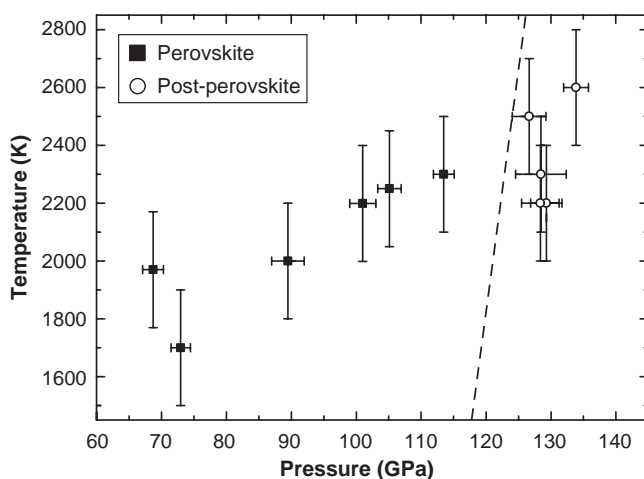| Crystal system	Orthorhombic		
Space group	*Cmcm*		
Cell parameters	a (Å)		2.456
	b (Å)		8.042
	c (Å)		6.093
	Z		4
	V (Å^3)		120.39
Atomic coordinates	x	y	z
Mg	0.000	0.253	0.250
Si	0.000	0.000	0.000
O1	0.000	0.923	0.250
O2	0.000	0.631	0.436
Interatomic distances (Å)			
Si-O		1.64 (×2), 1.66 (×4)	
Mg-O	1.84 (×2), 1.94 (×4), 2.13 (×2)		
Si-Si	2.46 (×2), 3.05 (×2), 3.11 (×2)		
Mg-Mg		2.46 (×2), 3.24 (×4)	

Fig. 3. Crystal structure of the post-perovskite phase projected along [001], [100], and [010] directions, and a stereoscopic view showing the layer-stacking structure. Coordination polyhedra of O atoms around Si atoms are shown as octahedra, and the Mg^{2+} ions are shown as balls. Bold line indicates the unit cell.
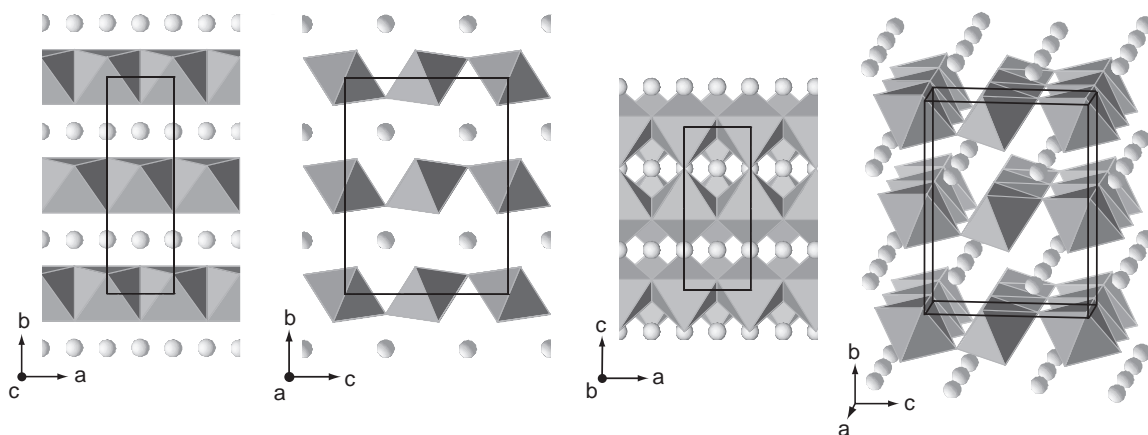
perovskite phase suggests slow longitudinal elastic-wave velocities propagating along the [010] direction. In addition, it is also inferred that the post-perovskite phase forms a platy crystal habit parallel to the (010) plane as a result of the sheet-stacking structure. A strong preferred orientation of such platy crystals may develop under the shear flow. A large S-wave polarization anisotropy ($V_{SH} > V_{SV}$) observed in the D″ region (1, 2) is possibly caused by the preferred orientation of the post-perovskite phase with the (010) plane being parallel to the horizontal shear flow, which is introduced by the down-welling of slabs and upwelling of plumes. This also provides an explanation for seismic anisotropy that is found only below the D″ discontinuity in the deep lower mantle.

References and Notes

1. B. J. Mitchell, D. V. Helmberger, *J. Geophys. Res.* **78**, 6009 (1973).
2. T. Lay, D. V. Helmberger, *Geophys. J. R. Astron. Soc.* **75**, 799 (1983).
3. M. E. Wysession *et al.*, in *The Core-Mantle Boundary Region*, M. Gurnis, M. E. Wysession, E. Knittle, B. A. Buffet, Eds. (American Geophysical Union, Washington, DC, 1998), vol. 28, pp. 273–297.
4. I. Sidorin, M. Gurnis, D. V. Helmberger, *Science* **286**, 1326 (1999).
5. E. Knittle, R. Jeanloz, *Science* **235**, 668 (1987).
6. G. Serghiou, A. Zerr, R. Boehler, *Science* **280**, 2093 (1998).
7. G. Fiquet, A. Dewaele, D. Andrault, M. Kunz, T. Le Bihan, *Geophys. Res. Lett.* **27**, 21 (2000).
8. R. M. Wentzcovitch, J. L. Martins, G. D. Price, *Phys. Rev. Lett.* **70**, 3947 (1993).
9. L. Stixrude, R. E. Cohen, *Nature* **364**, 613 (1993).
10. M. C. Warren, G. J. Ackland, B. B. Karki, S. J. Clark, *Mineral. Mag.* **62**, 585 (1998).
11. S. H. Shim, T. S. Duffy, G. Shen, *Science* **293**, 2437 (2001).
12. C. Meade, H. K. Mao, J. Hu, *Science* **268**, 1743 (1995).
13. S. K. Saxena *et al.*, *Science* **274**, 1357 (1996).
14. H. K. Mao, G. Shen, R. J. Hemley, *Science* **278**, 2098 (1997).
15. XRD spectra were collected on an imaging plate with an exposure time of 1 to 5 min. A monochromatic incident x-ray beam with a wavelength of 0.4134 or 0.4136 Å was collimated to 20 μm in diameter. The two-dimensional XRD image was integrated as a function of 2θ in order to give a conventional one-dimensional diffraction profile.
16. M. Murakami, K. Hirose, S. Ono, Y. Ohishi, *Geophys. Res. Lett.* **30**, 11 (2003).
17. S. Ono, K. Hirose, M. Isshiki, K. Mibe, Y. Saito, *Phys. Chem. Miner.* **29**, 527 (2002).
18. G. Shen, H. K. Mao, R. J. Hemley, in *Proceedings of the 3rd NIRIM International Symposium on Advanced Materials* (National Institute for Research in Inorganic Materials, Tsukuba, Japan, 1996), pp. 149–152.
19. T. Watanuki, O. Shimomura, T. Yagi, T. Kondo, M. Isshiki, *Rev. Sci. Instrum.* **72**, 1289 (2001).
20. J. C. Jamieson, J. N. Fritz, M. H. Manghnani, in *High Pressure Research in Geophysics*, S. Akimoto, M. H. Manghnani, Eds. (Reidel, Boston, 1982).
21. S. H. Shim, T. S. Duffy, G. Shen, *Phys. Earth Planet. Int.* **120**, 327 (2000).
22. T. Uchida, N. Funamori, K. Oguri, Y. Nakamura, T. Yagi, *Rev. High Press. Sci. Technol.* **5**, 261 (1996).
23. D. H. Xiong, L. C. Ming, M. H. Manghnani, *Phys. Earth Planet. Int.* **43**, 244 (1986).
24. The MD calculations were carried out with the full Ewald method for electrostatic interactions, the velocity Verlet algorithm with a 2-fs time step for integration of equations of motions of atoms, and constant number of atoms-volume-temperature (NVT) and constant number of atoms-temperature-pressure (NTP) ensembles. The interatomic potential

model used in the calculation was prepared to well reproduce the perovskite-type $MgSiO_3$ structure at 300 K (observed $a = 4.325$ Å, $b = 4.579$ Å, and $c = 6.308$ Å; calculated $a = 4.403$ Å, $b = 4.574$ Å, and $c = 6.410$ Å at 109 GPa).
25. G. Fiquet *et al.*, *Phys. Earth Planet. Int.* **105**, 21 (1998).
26. P. H. Noël, J. Padiou, *Acta Crystallogr.* **B32**, 1593 (1976).
27. I. Sidorin, M. Gurnis, D. V. Helmberger, *J. Geophys. Res.* **104**, 15005 (1999).
28. G. Masters, D. Gubbins, *Phys. Earth Planet. Int.* **140**, 159 (2003).
29. Y. Fei, *Am. Mineral.* **84**, 272 (1999).
30. We thank Y. Tatsumi, T. Tsuchiya, D. Yuen, J. Tuff, and Y. Kuwayama for discussions. In situ x-ray measure-ments were conducted at SPring-8 (proposal no. 2002B0537-ND2-np and 2003A0013-LD2-np). M.M. was supported by the Japan Society for the Promotion of Science (JSPS) Research Fellowships for Young Scientists.

Degradation of Terrigenous Dissolved Organic Carbon in the Western Arctic Ocean

Dennis A. Hansell,[1]* David Kadko,[1] Nicholas R. Bates[2]

The largest flux of terrigenous organic carbon into the ocean occurs in dissolved form by way of rivers. The fate of this material is enigmatic; there are numerous reports of conservative behavior over continental shelves, but the only knowledge we have about removal is that it occurs on long unknown time scales in the deep ocean. To investigate the removal process, we evaluated terrigenous dissolved organic carbon concentration gradients in the Beaufort Gyre of the western Arctic Ocean, which allowed us to observe the carbon's slow degradation. Using isotopic tracers of water-mass age, we determined that terrigenous dissolved organic carbon is mineralized with a half-life of 7.1 ± 3.0 years, thus allowing only 21 to 32% of it to be exported to the North Atlantic Ocean.

Terrigenous dissolved organic carbon (tDOC) enters the global ocean by way of rivers at a rate of ~0.25 Pg C yr^{-1} (1), constituting the largest transfer of reduced carbon from the continents to the open ocean. The fate of this material once it is delivered to the ocean remains uncertain. Studies that use salinity-DOC relationships across the world's estuaries and ocean margins show conservative tDOC behavior (1, 2), suggesting a long-lived material. In contrast, low concentrations of tDOC tracers in the open ocean (e.g., lignin and stable isotopic compositions) (3, 4) indicate active removal processes, but the time and space scales of the processes remain unknown.

On a per volume basis, the Arctic Ocean receives the greatest loads of terrestrial fresh water and organic matter of any ocean. Rivers draining into the Arctic Ocean comprise ~10% of the global river flux and have high DOC content (5), typically >600 μM C. This material is long lived, such that up to ~25% of the DOC in the surface central Arctic consists of terrigenous components (6, 7). Previous studies that have used DOC-salinity relationships in the

eastern Arctic Ocean (e.g., the Eurasian Basin and its bordering seas) have indicated that tDOC in fluvial water mixes conservatively with marine water over the continental margins (8, 9), yet <50% of the tDOC entering the Arctic Ocean survives for export to the North Atlantic (6, 10).

The gyre circulation of the western Arctic Ocean (i.e., the Canada Basin and adjacent continental shelf seas) provides the conditions necessary for observing substantial tDOC removal over decadal time scales. In this study, physical and biogeochemical measurements were made from the *USCGC Healy* during a spring cruise (5 May to 15 June 2002; sea-ice cover >90%) to the Chukchi Sea as part of the Western Arctic Shelf-Basin Interactions (SBI) project (11). Thirty-nine stations, largely on three meridional sections, were occupied on the Chukchi Sea shelf and in the adjacent Arctic Ocean basin (Fig. 1). The parts of the sections that are located over the continental shelf largely comprised water of Pacific Ocean origin (by way of the Bering Strait). Present at the northern end of the sections, over the deep Canada Basin, was the polar surface layer (PSL), an ice-covered, relatively low-salinity water mass that is a mix of riverine waters (~8 m of meteoric water in the upper 40 m) (12) and marine waters (13). The upper few hundred meters of the Arctic Ocean are strongly strati-

[1]Rosenstiel School of Marine and Atmospheric Science, University of Miami, Miami, FL 33149, USA. [2]Bermuda Biological Station for Research, 17 Biological Lane, Ferry Reach, St. George's GE-01, Bermuda.

*To whom correspondence should be addressed. E-mail: dhansell@rsmas.miami.edu